Source of the low-altitude hiss in the ionosphere

Lunjin Chen, Ondřej Santolík, Mychajlo Hajoš, Liheng Zheng, Zeren Zhima, Roderick Heelis, Miroslav Hanzelka, Richard B. Horne, Michel Parrot

AGU PUBLICATIONS

Geophysical Research Letters

RESEARCH LETTER
10.1002/2016GL072181

Key Points:
- The observed characteristics of low-altitude hiss in the ionosphere are presented
- Whistler mode in the magnetosphere serves as the source for the low-altitude hiss in the ionosphere
- The mechanisms for accessibility to the ionosphere have been identified for explaining the observed features of the low-altitude hiss

Correspondence to:
L. Chen,
lunjin.chen@gmail.com

Citation:
Chen, L., O. Santolík, M. Hajoš, L. Zheng, Z. Zhima, R. Heelis, M. Hanzelka, R. B. Horne, and M. Parrot (2017), Source of the low-altitude hiss in the ionosphere, *Geophys. Res. Lett.*, *44*, 2060–2069, doi:10.1002/2016GL072181.

Received 6 DEC 2016
Accepted 23 JAN 2017
Accepted article online 27 JAN 2017
Published online 3 MAR 2017

Source of the low-altitude hiss in the ionosphere

Lunjin Chen[1], Ondrej Santolík[2,3], Mychajlo Hajoš[3], Liheng Zheng[1], Zeren Zhima[1], Roderick Heelis[1], Miroslav Hanzelka[2,3], Richard B. Horne[4], and Michel Parrot[5]

[1]William B. Hanson Center for Space Sciences, University of Texas at Dallas, Richardson, Texas, USA, [2]Department of Space Physics, Institute of Atmospheric Physics, Prague, Czech Republic, [3]Faculty of Mathematics and Physics, Charles University in Prague, Prague, Czech Republic, [4]British Antarctic Survey, Natural Environment Research Council,Cambridge, UK, [5]LPC2E/CNRS, Orléans, France

Abstract We analyze the propagation properties of low-altitude hiss emission in the ionosphere observed by DEMETER (Detection of Electromagnetic Emissions Transmitted from Earthquake Regions). There exist two types of low-altitude hiss: type I emission at high latitude is characterized by vertically downward propagation and broadband spectra, while type II emission at low latitude is featured with equatorward propagation and a narrower frequency band above $\sim f_{cH+}$. Our ray tracing simulation demonstrates that both types of the low-altitude hiss at different latitude are connected and they originate from plasmaspheric hiss and in part chorus emission. Type I emission represents magnetospheric whistler emission that accesses the ionosphere. Equatorward propagation associated with type II emission is a consequence of wave trapping mechanisms in the ionosphere. Two different wave trapping mechanisms are identified to explain the equatorial propagation of Type II emission; one is associated with the proximity of wave frequency and local proton cyclotron frequency, while the other occurs near the ionospheric density peak.

1. Introduction

Plasmaspheric hiss is an incoherent, broadband, electromagnetic whistler mode emission preferentially and steadily observed inside the high-density plasmasphere [*Russell et al.*, 1969; *Thorne et al.*, 1973] and storm time plasmaspheric plume [*Summers et al.*, 2008]. Plasmaspheric hiss has a typical frequency range from ~100 Hz and ~2 kHz [*Thorne et al.*, 1973; *Meredith et al.*, 2004], with most power between ~200 Hz and 1 kHz [*Smith et al.*, 1974; *Hayakawa and Sazhin*, 1992]. Recent ray tracing simulations [*Chum and Santolík*, 2005; *Santolík et al.*, 2006a; *Bortnik et al.*, 2008] and observations [*Bortnik et al.*, 2009] have suggested that plasmaspheric hiss originates from chorus emission generated outside the plasmasphere. This mechanism can account for plasmaspheric hiss in the typical frequency range 200–2000 Hz as well as many other characteristic features [*Chen et al.*, 2012a, 2012b], including the spatial distribution and intensity of the observed plasmaspheric hiss. The contribution of local growth to the hiss emission is also discussed [e.g., *Chen et al.*, 2014; *Omura et al.*, 2015].

The low-altitude hiss is an electromagnetic emission in the ionosphere in the frequency range of 100 Hz to 1 kHz (close to the local proton cyclotron frequency) and has been often observed from Freja and DEMETER (Detection of Electromagnetic Emissions Transmitted from Earthquake Regions) spacecraft. Previous propagation analysis has shown that the emissions at high latitudes have vertically downward propagation directions in both hemispheres, which turn slightly poleward and equatorward at higher and lower latitudes, respectively [e.g., *Santolík and Parrot*, 1999, 2000; *Santolík et al.*, 2006a]. Similar propagation features are also present for quasiperiodic emission [*Hayosh et al.*, 2016], which propagates equatorward at low latitudes. It has been suggested that the low-altitude hiss emissions at high latitudes are an ionospheric manifestation of magnetospheric whistler mode chorus [e.g., *Santolík and Parrot*, 1999; *Santolík et al.*, 2006a]. However, it remains a question of how to reconcile the dependence of the low-altitude hiss propagation directions on magnetic latitude. In this study, we will address this question to understand the physical mechanism responsible for propagation of the low-altitude hiss from high to low latitudes. We will illustrate an example of the low-altitude hiss observed by DEMETER spacecraft in section 2. We will use ray tracing techniques to simulate propagation characteristics of magnetospheric whistler mode emission, in particular plasmaspheric hiss, in both the magnetosphere and the ionosphere in section 3, followed by conclusions and discussion in section 4.

2. DEMETER Observation

DEMETER, a French satellite launched by Centre National des Etudes Spatiales in June 2004, was a low-altitude and three-axis stabilized satellite following a nearly Sun-synchronous circular orbit (10:30 and 22:30 LT). The initial altitude of the spacecraft (710 km) was decreased to 660 km in December 2005 [*Parrot et al.*, 2006]. The mission came to the end in December 2010, meaning that about 6.5 years of measured data are available. The ICE (Instrument Champ Electrique) [*Berthelier et al.*, 2006], equipped with electric antennas of four 30 mm spheres on 4.5 m boom, provides electric field instrument. The magnetic field measurement is provided by the three-axial search coil magnetometer IMSC [*Parrot et al.*, 2006]. In their ELF frequency range (up to 1 kHz), waveforms of all six components of the electromagnetic field have been collected with sampling frequency 2.5 kHz, allowing us to analyze the propagation and polarization properties of the observed electromagnetic waves. The intercalibration was done before launch and verified in flight [*Santolík et al.*, 2006b].

Figure 1 shows low-altitude electromagnetic hiss emissions and associated propagation properties recorded by DEMETER during one of the dayside orbits (magnetic local time (MLT) ~10) on 13 March 2008, for the Northern Hemisphere (Figures 1a–1f) and subsequent Southern Hemisphere (Figures 1g–1l) passage. The observed waveforms have been analyzed using a 512-point fast Fourier transform, and multicomponent 6×6 spectral matrices have been obtained. Based on these spectral matrices, we have determined the ellipticity of the magnetic field polarization, the wave vector direction, and the Poynting vector direction [*Santolík et al.*, 2010, and references within]. The emissions observed in both hemispheres show great symmetry about the magnetic equator, which will be summarized shortly. By examination of the north passage (Figures 1a–1f), one can notice two types of electromagnetic emissions. The first type, type I, is observed at relatively high latitude ($\lambda > \sim 55°$), characterized by a broad frequency range from ~300 Hz to 800 Hz (Figures 1a and 1b), right-handed polarization (Figure 1e), nearly vertically downward direction for both propagation vector **K** (Figures 1c and 1d), and Poynting vector **P** (Figure 1f). The vertically downward propagation direction is based on the following observations: (1) the background magnetic field **B** direction at high-latitude ionosphere has a nearly vertical direction, (2) the wave normal angle between propagation vector and background magnetic field θ_{BK} is close to 0° (Figure 1c), and (3) the azimuth angle of **K**, ϕ_{BK}, is close to 180° (Figure 1d), meaning that **K** is oriented toward the Earth. Here ϕ_{BK} is defined as the azimuthal angle of **K** with respect to **B** with a value of 0° (180°) denoting directions in the meridian plane toward increasing (decreasing) *L* shell direction. Similar **P** direction can be extracted by $\theta_{BP} \sim 0°$ (Figure 1f) and $\phi_{BP} \sim 180°$ (not shown), where the definitions of the angles between the magnetic field and the Poynting vector (**P**), θ_{BP} and ϕ_{BP}, are similar to θ_{BK} and ϕ_{BK} for the **K** direction.

In comparison with type I emission, the second type II of the emission is observed at lower latitudes, with a narrower frequency range (of width ~200 Hz) in vicinity of local proton cyclotron frequency f_{ch} (white lines in Figures 1a and 1b) and a mixed ellipticity ranging from a right-handed, nearly circular polarization near the upper frequency limit and a linear and even left-handed polarization toward the lower frequency limit (Figure 1e), which is below f_{ch}. The **K** direction of type II is nearly perpendicular to the background magnetic field and toward decreasing latitudes, based on the analysis that $\theta_{BK} \sim 90°$ and $\phi_{BK} \sim 180°$ (Figures 1c and 1d). Poynting vector **P** of type II follows a similar perpendicular direction as **K** (Figure 1f).

The type I and type II emissions are also observed during the subsequent Southern Hemisphere passage (Figures 1g–1l), with a great degree of symmetry about the magnetic equator. The propagation properties are summarized in Figure 1m, with the type I emission of vertically downward propagation and the type II emission toward the equator on both hemispheres. Such propagation routes reasonably spark a speculation that type I emission may originate from the magnetosphere at higher altitude and then turn into type II emission in the ionosphere. That is, despite different observed characteristics, type I and type II emissions are the same emissions at different latitudes in the ionosphere and both originate from a common magnetospheric emission. A possible candidate for the emission source is magnetospheric whistler mode emission, in particular plasmaspheric hiss, because (1) plasmaspheric hiss has similar frequency range as type I and (2) type I can be seen down to a lower *L* value of 4. To verify this speculation, we will investigate propagation characteristics of plasmaspheric hiss using a ray tracing technique to describe the accessibility to the low-altitude ionosphere, which will be presented in the next section.

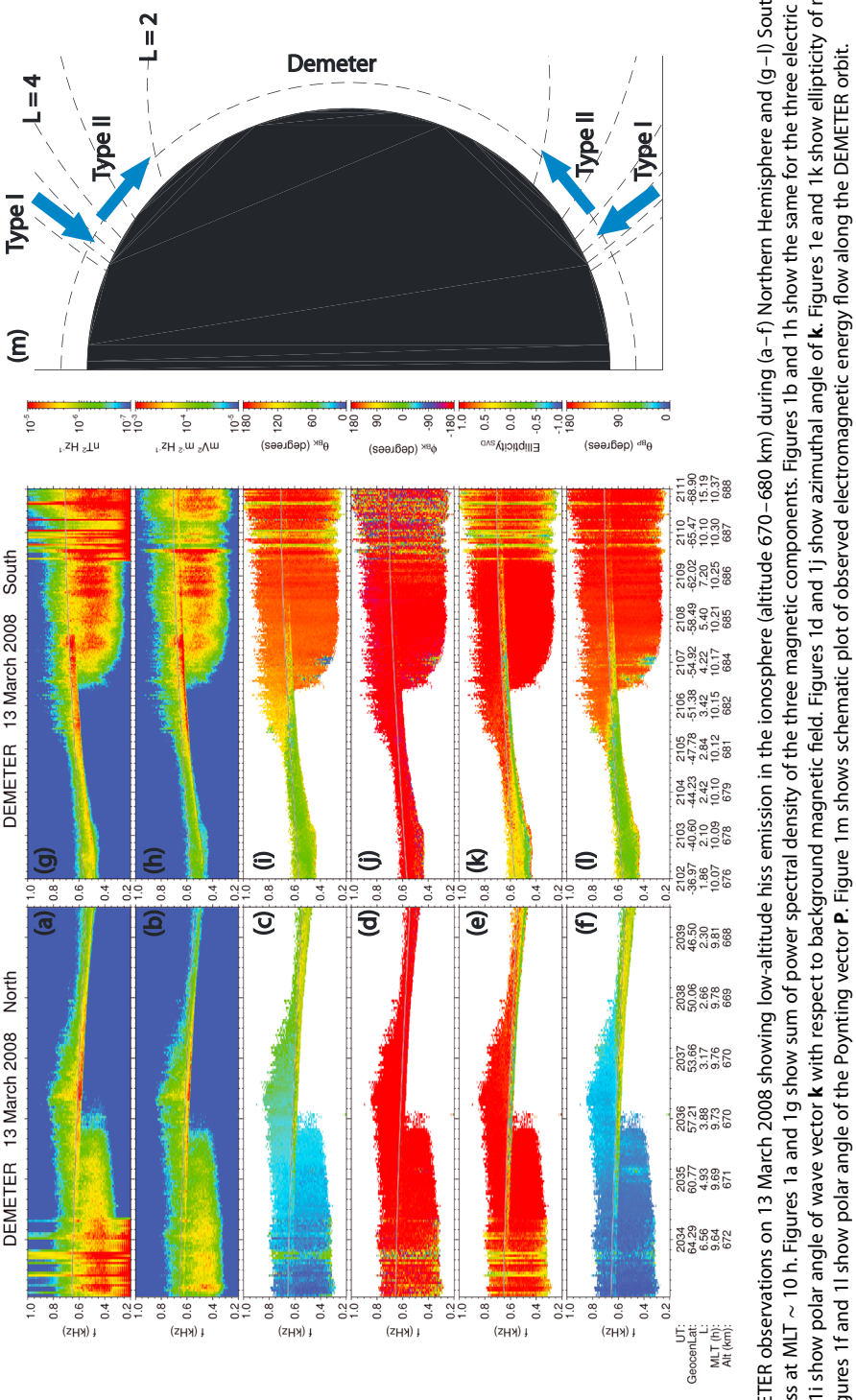

Figure 1. DEMETER observations on 13 March 2008 showing low-altitude hiss emission in the ionosphere (altitude 670–680 km) during (a–f) Northern Hemisphere and (g–l) Southern Hemisphere pass at MLT ~ 10 h. Figures 1a and 1g show sum of power spectral density of the three magnetic components. Figures 1b and 1h show the same for the three electric components. Figures 1c and 1i show polar angle of wave vector **k** with respect to background magnetic field. Figures 1d and 1j show azimuthal angle of **k**. Figures 1e and 1k show ellipticity of magnetic field polarization. Figures 1f and 1l show polar angle of the Poynting vector **P**. Figure 1m shows schematic plot of observed electromagnetic energy flow along the DEMETER orbit.

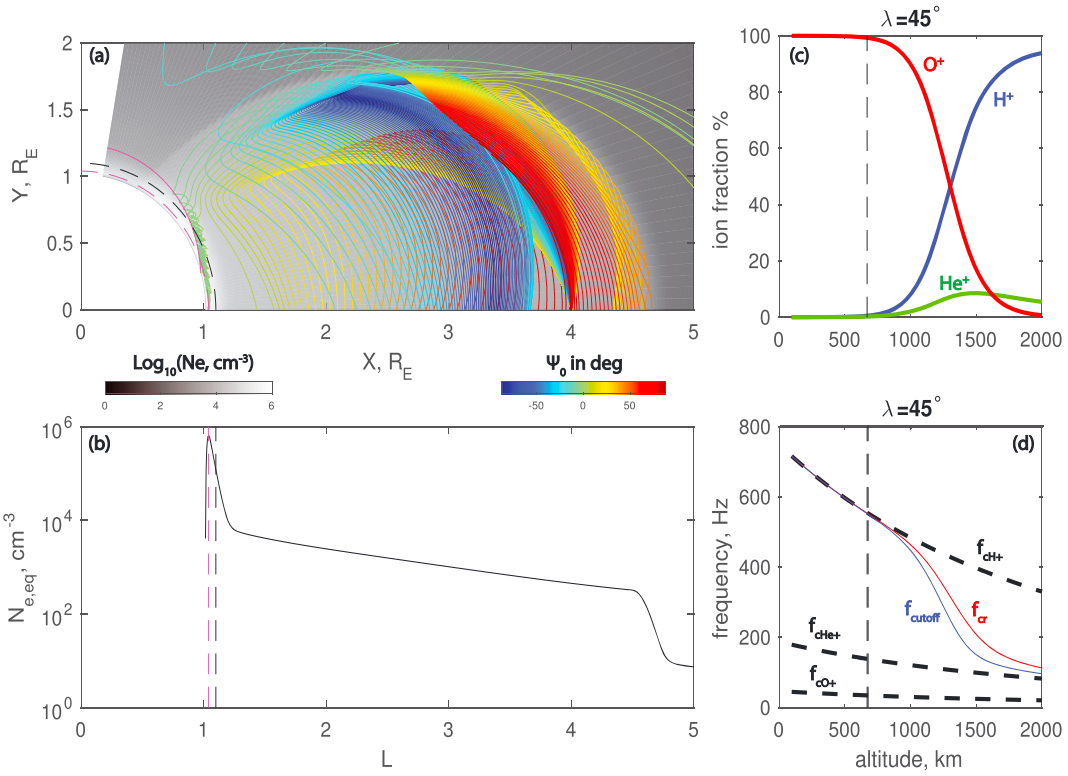

Figure 2. (a) Ray tracing results for plasmaspheric hiss waves launched at $L = 4$ with wave frequency $f = 500$ Hz and a full range of initial wave normal angle $-88° \le \psi_0 \le 88°$ (indicated by color) with spacing of 1°. The gray color background denotes electron density variation in the meridian plane used for the ray tracing simulation. Also denoted are the contour of $f_c h = 500$ Hz (solid magenta line), ionospheric density peak (the dashed magenta line), and the altitude of DEMETER satellite (the black dashed line). (b) Equatorial profile of electron density used in ray tracing model. (c) Ion fractions as a function of altitude at magnetic latitude $\lambda = 45°$. (d) Characteristic frequencies as a function of altitude at $\lambda = 45°$.

3. Ray Tracing Model

To model the propagation characteristics of plasmaspheric hiss waves, we use the HOTRAY ray tracing code [*Horne*, 1989], where a magnetic dipole field and a diffusive equilibrium plasma density model [*Bortnik et al.*, 2011, and references within] are adopted. The plasmapause inner edge is set to $L = 4.5$ with a width of ~0.3 R_E, where R_E is the Earth radius, and the ionospheric density peak of $\sim 10^6$ cm^{-3} remains at an altitude of 250 km (magenta dashed lines of Figures 2a and 2b). The electron density variation in the meridian plane is shown in Figure 2a by the gray color scale, and the equatorial electron density distribution is shown in Figure 2b. The DEMETER altitude (black dashed line) is on the topside of ionospheric density distribution, where there is a rather strong negative density gradient in the radial direction (Figure 2b). Since the wave frequency of interest is close to the ion cyclotron frequency, wave propagation characteristics will be affected by ion (H^+, He^+, and O^+) composition, which is shown in Figure 2c as a function of altitude at constant latitude $\lambda = 45°$. In the magnetosphere, H^+ ions are the predominant species due to the lightest mass and thus highest scale height, while ions can be dominated by O^+ in the ionosphere, because of the presence of more oxygen atoms to be ionized. Corresponding to Figure 2c, Figure 2d shows characteristic frequencies in a magnetized plasma of multiple ions, including three ion gyrofrequencies (f_{cH+}, f_{cHe+}, and f_{cO+}), the crossover frequency f_{cr}, and the cutoff frequency f_{cutoff} between f_{cHe+} and f_{cH+}. As altitude decreases, H^+ ion concentration decreases and as a result f_{cr} and f_{cutoff} tend to merge to have the value of f_{cH+}. One can notice that those three characteristic frequencies (f_{cH+}, f_{cr}, and f_{cutoff}) are close to the frequency range of the low-altitude hiss emission seen by DEMETER.

A 2-D ray tracing simulation is performed to study the accessibility of plasmaspheric hiss to the low-altitude, low-latitude ionosphere. Two-dimensional simulation is justified because the observed low-altitude hiss from DEMETER is mostly confined to ±30° of a meridian plane. Figure 2a shows raypaths of plasmaspheric hiss

waves launched at the equator $L = 4$ with a fixed frequency of 500 Hz and a full range of initial wave normal angle direction ψ_0 from −88° to +88° with a spacing of 1°. Wave vectors of negative ψ points toward smaller L shell, while those of positive values point toward larger L shell, which corresponds to ϕ_{BK} =180° and 0°, respectively. Most of rays experience reflection from the steep plasmapause or magnetospheric reflection, and consequently, they are confined within the plasmasphere. The magnetospheric reflection is a typical phenomenon for whistler mode propagation in the magnetosphere. That is, as the whistler mode propagates toward higher latitude, the wave normal angle turns through 90° quickly when the wave frequency is below the local lower hybrid resonant frequency, leading to reflection toward lower latitude. There exists, however, a fraction of emission that leaves the plasmasphere and leaks partially outside toward the plasma trough region of higher L and partially inside toward the low-altitude ionosphere. The former leaked emission likely experiences rapid attenuation through strong Landau damping due to suprathermal electrons, while the latter can survive for a longer time except at the region where accumulated collisional damping becomes significant. One can see that the plasmaspheric hiss emissions with initial ψ_0 in the range of (−41°, −45°) propagate vertically downward toward the ionosphere without experiencing magnetospheric reflection and subsequently turn toward lower latitude inside the ionosphere. During the equatorward propagation, those raypaths are mostly confined in a radially narrow region outside the local proton gyrofrequency contour of 500 Hz (solid magenta line), meaning that those emissions can only be available when the wave frequency is above the local proton gyrofrequency. This is consistent with the DEMETER observation (Figures 1a and 1b), showing the lack of type II emission in the frequency range below approximately the local proton gyrofrequency. This behavior was also confirmed by an independent ray tracing simulation using the same method as *Santolík et al.* [2006a], with a verification of the Wentzel-Kramers-Brillouin approximation of geometric optics. This approximation fails for reflection at the lower altitude where we can assume a specular reflection of the ray instead of its refraction.

The detailed propagation characteristics are examined in Figure 3 for one of those rays with initial $\psi_0 = -43°$. Figure 3a shows the raypath with wave vector directions denoted by black line segments, and Figure 3b shows an expanded view in the low-altitude region. The temporal variation of the wave normal angle ψ, normalized frequency f/f_{cH+}, the ratio of plasma to electron gyrofrequency f_{pe}/f_{ce}, and the electric polarization is shown in Figures 3c–3f, respectively. A condition for plasmaspheric hiss emission to access the low-altitude ionosphere is that magnetospheric reflection should not take place in the plasmasphere. That is, the wave normal should remain quasi-parallel during propagation toward high latitude. The wave normal of this ray, which initially points toward decreasing L, becomes field aligned and then points toward increasing L (Figure 3a), primarily because of dipole magnetic field refraction. As the ray approaches the plasmapause, the strong density gradient near the plasmapause produces inward refraction, which exceeds outward refraction due to the magnetic field, leading to inward turning of the wave normal direction (Figure 3c). Through comparable inward and outward refraction, the wave normal angle does not turn toward 90° inside the plasmasphere (Figure 3c). This results in propagation toward the ionosphere (Figure 3a) with a relatively small wave normal angle (Figure 3c), which is consistent with DEMETER observation of type I emission (Figure 1).

When inside the ionosphere (Figure 3b), this ray propagates toward lower latitude and slowly toward lower altitude while experiencing two kinds of wave trapping. Such wave trapping allow the ray to stay in the ionospheric altitude range rather than returning to the plasmasphere and to propagate from high to low latitudes, which accounts for equatorial propagation characteristics of type II emission mentioned above. The first kind of wave trapping is characterized by the following five points.

1. There exists a lower altitude limit marked by a contour of local proton cyclotron frequency equal to the wave frequency (magenta solid line of Figure 3b).
2. There exists a lower normalized frequency limit at local f_{cutoff} (Figure 3d), which here is close to local f_{cH+} due to low H^+ concentration.
3. The wave normal oscillates about the direction perpendicular to the background magnetic field (Figure 3c), with $\psi \sim -90°$.
4. A mixed polarization is seen in Figure 3f from right-handed polarization when $f > f_{cr}$, linear polarization when $f \sim f_{cr}$, and left-handed polarization when $f < f_{cr}$.
5. As the ray approaches the lower altitude limit and the frequency approaches f_{cutoff}, the ray group velocity slows down, which can be seen by quasi-constant f_{pe}/f_{ce} and f/f_{cH+} over a few intervals of 1–2 s duration. In contrast, reflection at the upper altitude limit is faster, indicated by narrow peaks in f/f_{cH+} (Figure 3d) and narrow dips in f_{pe}/f_{ce} (Figure 3e) over intervals of a fraction of a second.

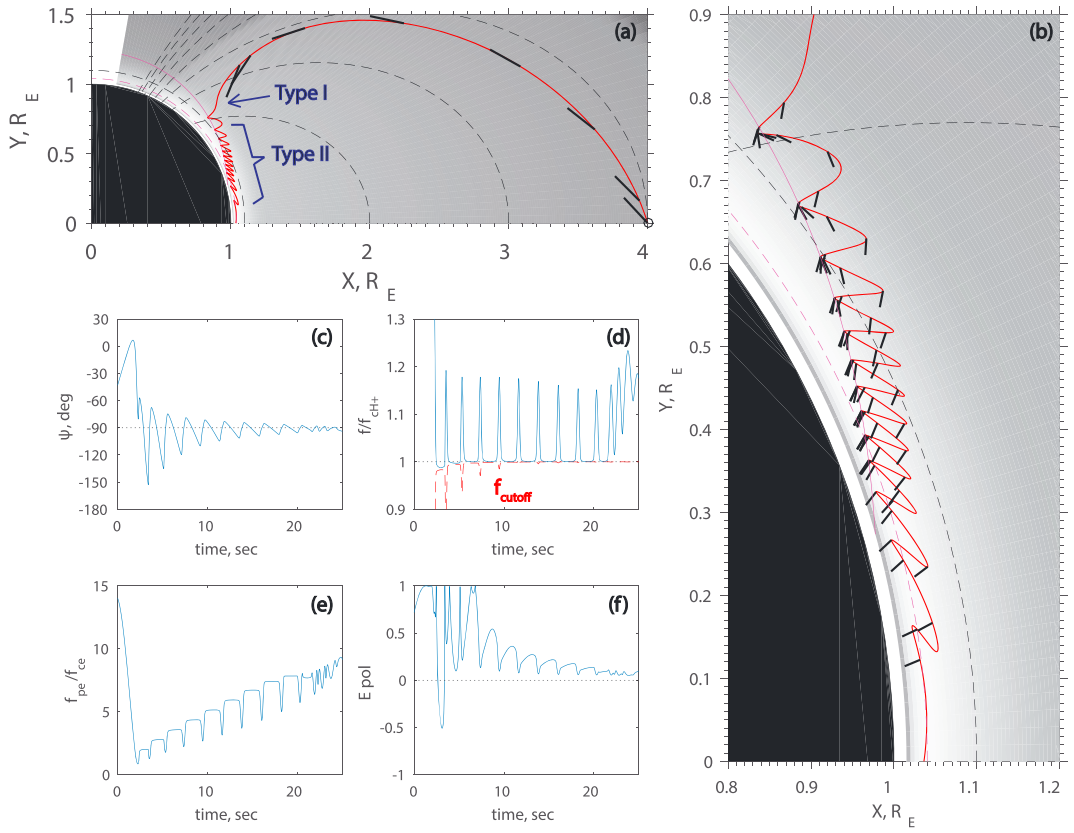

Figure 3. An example of ray tracing results in Figure 2a with $\psi_0 = -43°$. (a) A raypath in a similar format to Figure 2a. Black line segments along the raypath denotes local **k** direction variation. (b) A zoom-in plot in the low-altitude range. (c–f) The variation along the propagation path of wave normal angle ψ, normalized wave frequency to local f_{ch}, the ratio of f_{pe}/f_{ce}, and electric field polarization with 1 defined as circularly right handed, 0 as linear polarization, and −1 as circularly left handed polarization.

The second kind of wave trapping features an oscillatory raypath centered at the ionospheric density peak (magenta dashed line), $\psi \sim -90°$ with slightly right handed and linear polarization. The wave reflects at the upper and lower sides of the density peak, with density gradients both pointing toward the peak.

To understand the two wave trapping mechanisms, we resort to the optic principle, Snell's law. We start with examining the whistler mode refractive index $n = kc/\omega$ in a cold magnetic plasma, where k is the wave number magnitude, c is the speed of light, and ω is the wave angular frequency. Figure 4a shows the dependence of the refractive index as a function of normalized wave frequency f/f_{cH+}, for different values of wave normal angles, f_{pe}/f_{ce}, and H^+ concentration, respectively. The refractive index peaks at wave normal angle $\psi = 90°$ and tends to increase with f/f_{cH+} and f_{pe}/f_{ce}. The refractive index for $\psi = 90°$ decreases as f/f_{cH+} decreases and drops steeply to zero as f approaches the cutoff frequency f_{cutoff}, where the group velocity also approaches zero. This explains why the reflection at the lower altitude boundary takes place slowly for the first wave trapping mechanism. For lower H^+ concentration (the black line), f_{cutoff} is closer to f_{cH+} and thus the refractive index shows a sensitive frequency dependence near f_{cH+}.

Figure 4b schematically explains the first wave trapping mechanism at high latitude using the *Poeverlein* [1950] graphical construction. From top to bottom panels, refractive index surfaces from high altitude to low altitude are plotted. A few simplifications are made. First, the magnetic field line is assumed to be in the vertical direction. Second, we assume that plasma density spatial inhomogeneity primarily causes the wave refraction (wave number vector variation) and the inhomogeneity is along the vertical direction so that according to Snell's law, the horizontal component of the wave vector is conserved. As the wave propagates upward toward the upper reflection boundary (that is, farther away from the ionospheric density peak), the refractive index surface shrinks due to decreasing f_{pe}/f_{ce}. As a consequence, the wave vector turns 90° according to Snell's law, leading to wave reflection toward the lower altitude. During wave downward propagation, the refractive

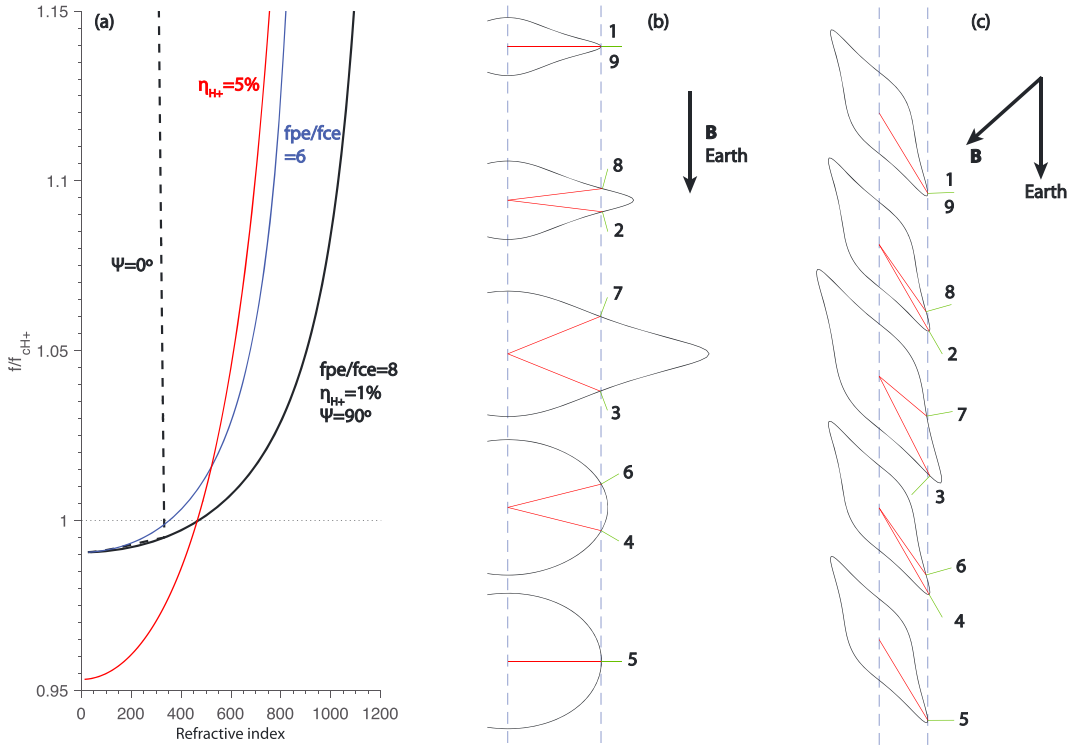

Figure 4. (a) Dependence of refractive index on wave normalized frequency, wave normal angle, plasma density, and ion fraction. The nominal case (ψ = 90°, f_{pe}/f_{ce} = 8, and η_{H+} = 1%) is shown by the black solid line. The labels next to other lines represent the changed parameters compared with the nominal case. Schematic plot to illustrate variation of refractive index surface for two types of wave trapping mechanisms, (b) through balance between reflection near f_{cutoff} and negative radial gradient of plasma density and (c) through positive and negative radial gradient on the two sides of the ionospheric density peak. The red and green segments represent the wave normal direction and the group velocity direction, respectively, during a sequence of the wave trapping process labeled by the numbers.

index surface enlarges (due to increasing f_{pe}/f_{ce}) and the wave normal moves away from the perpendicular direction. As the wave propagates farther downward, the refractive index surface shrinks again and become more isotropic as the frequency gets closer to f_{cutoff}, leading to wave normal turning perpendicular and wave reflection at the lower altitude.

Figure 4c schematically explains the second wave trapping mechanism due to gradients in the plasma density, where waves are trapped near the ionospheric density peak. Again, from the top to bottom, refractive index surfaces for altitudes above the density peak, at the density peak, and below the density peak are plotted. We still assume that plasma spatial inhomogeneity primarily causes the wave refraction (wave number vector variation) and the inhomogeneity is along the vertical direction so that according to Snell's law, the horizontal component of the wave vector is conserved. We also assume a constant magnetic field direction (but not necessarily in vertical direction since this type of wave trapping mechanism can occur near the equatorial region). The variation in refractive index surface is caused by the variation of plasma density (thus f_{pe}/f_{ce}). When the wave propagates away from the ionospheric density peak, the refractive index shrinks, leading to wave reflection on both sides.

We also simulate raypaths of plasmaspheric hiss launched from different equatorial locations that correspond to a typical L range ($L > 2$) of intense plasmaspheric hiss [*Chen et al.*, 2012b]. Figure 5 only shows raypaths that can access ionospheric altitudes (<0.3 R_E). Among them, rays in the solid lines can subsequently be trapped in the ionosphere and propagate equatorward while rays in the dotted lines cannot. One can notice that ionospheric latitude ranges just below the plasmapause are preferred for plasmaspheric hiss to access the ionosphere. Plasmaspheric hiss from different equatorial regions can contribute a fraction of wave power in those latitudes, where propagation vector direction are preferentially downward. Some of those rays are able to propagate equatorward in the ionosphere. For wave trapping inside the ionosphere to happen, refraction away from the plasmapause is required. We also check the ionospheric accessibility of magnetospheric chorus

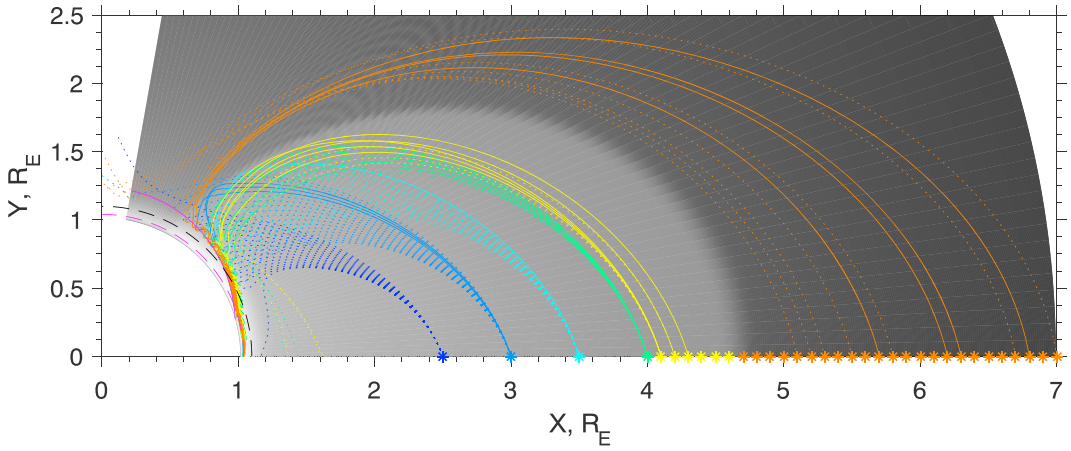

Figure 5. Dependence of whistler mode raypaths on equatorial launching location. The simulation is done for various equatorial locations (indicated by asterisk symbols) for $f = 500$ Hz over a full range of ψ_0 of 1° spacing. Only raypaths that can reach below an altitude of 0.3 R_E are shown, with solid lines and dotted lines representing those rays that can and cannot undergo wave trapping in the ionosphere, respectively.

wave emission outside the plasmasphere (orange lines). A fraction of chorus waves can also access the ionosphere and turn equatorward in the ionosphere after significant inward refraction by the plasmapause.

The model results show consistencies with DEMETER observations and allow us to interpret type I and type II emission in the following way. Type I emission represents the observation of downward propagation of chorus or plasmaspheric hiss that is capable of accessing the ionosphere with small wave normal angles and can extend below f_{cH+} through the tunneling of right-handed polarized waves below the crossover frequency (also called H^+ and He^+ ion crossover frequency [*Santolík and Parrot*, 1998, 1999]). Type II emission represents equatorward propagation inside the ionosphere due to the wave trapping mechanisms described above. The first type wave trapping mechanism explains the equatorward direction of the wave normal vector and Poynting vector and the limit of wave frequency above f_{cutoff}, which is close to f_{cH+} in the ionosphere dominated by O^+ ion species. The wave trapping mechanism is also consistent with the presence of both downgoing and reflected upgoing waves by using the wave distribution function method [*Santolík and Parrot*, 2000]. The second kind of wave trapping occurs near the ionosphere density peak, which, however, cannot be seen by the DEMETER spacecraft.

4. Conclusions and Discussion

We present a propagation analysis of low-altitude hiss seen in DEMETER observations on the dayside. A ray tracing simulation is performed to demonstrate that a fraction of plasmaspheric hiss can leak out of the plasmasphere and access the ionosphere, which subsequently evolves into low-altitude hiss. Our principal conclusions are summarized as follows:

1. The observed low-altitude hiss waves possess vertically downward propagation vectors at high latitudes (type I), while at low latitude they turn equatorward with a narrower frequency range (type II).
2. Ray tracing simulations show that type I and type II emissions are part of the same low-altitude hiss emission in the ionosphere and that they can originate from plasmaspheric hiss and in part from chorus emission. The downward propagation occurs at the ionospheric access point, while the equatorward propagation is caused by wave trapping inside the ionosphere.
3. Two kinds of wave trapping mechanisms are identified to account for equatorward propagation characteristics of type II emission. The first kind wave trapping occurs just above f_{cutoff} on the negative gradient side of the ionospheric peak, while the second kind wave trapping occurs near the ionospheric density peak.
4. Trapping of equatorward propagating waves in the ionosphere requires refraction near the plasmapause before reaching the ionosphere.

We only investigate the propagation characteristics of magnetospheric whistler mode emission. Previous studies have demonstrated small Landau damping inside the plasmasphere, allowing a lifetime of ~30 s [*Chen et al.*, 2012a], and Landau damping outside the plasmasphere being low enough for allowing chorus waves

to propagate to high latitudes [*Bortnik et al.*, 2007]. Electron collisional damping can be significant in the *D* region [e.g., *Tao et al.*, 2010], which should not be a factor for our simulation, while ion collisional damping, which may be important, may accumulate to affect the late phase of wave trapping.

Ion composition in the ionosphere affects the lower frequency limit of type II emission, and the ionospheric density peak affects the wave trapping mechanisms. We might thus expect the frequency range of type II emission to be dependent on season and solar activity and latitude. In the winter hemisphere, during periods of low solar activity the relative contributions of H^+ and He^+ to the topside ion density will be increased. Furthermore, the contributions of He^+ is a strong function of latitude with a local peak near 20° magnetic latitude [*Li et al.*, 2015]. Thus, further evidence of the trapping mechanisms described here may be found by examining the relationships between the frequency range of the emission and the local ion composition in the ionosphere.

The low-altitude hiss is a counterpart of magnetospheric whistler mode, which plays important roles for radiation belt loss and acceleration. Understanding this accessibility of magnetospheric waves in the ionosphere may enable a valuable technique using ionospheric wave observation to monitor whistler mode wave activities above.

Acknowledgments
We acknowledge NSF grant 1405041 through the Geospace Environment Modeling program, the AFOSR grant FA9550-16-1-0344, National Capability funding from the UK Natural Environment Research Council, the GAČR17-07027S and LH15304 grants, and the Praemium Academiae award. DEMETER data are accessible from https://cdpp-archive.cnes.fr.

References

Berthelier, J. J., et al. (2006), ICE, the electric field experiment on DEMETER, *Planet. Space Sci.*, *54*, 456–471, doi:10.1016/j.pss.2005.10.016.
Bortnik, J., R. M. Thorne, and N. P. Meredith (2007), Modeling the propagation characteristics of chorus using CRRES suprathermal electron fluxes, *J. Geophys. Res.*, *112*, A08204, doi:10.1029/2006JA012237.
Bortnik, J., R. M. Thorne, and N. P. Meredith (2008), The unexpected origin of plasmaspheric hiss from discrete chorus emissions, *Nature*, *452*, 62–66, doi:10.1038/nature06741.
Bortnik, J., W. Li, R. M. Thorne, V. Angelopoulos, C. Cully, J. Bonnell, O. Le Contel, and A. Roux (2009), An observation linking the origin of plasmaspheric hiss to discrete chorus emissions, *Science*, *324*, 775–778, doi:10.1126/science.1171273.
Bortnik, J., L. Chen, W. Li, R. M. Thorne, and R. B. Horne (2011), Modeling the evolution of chorus waves into plasmaspheric hiss, *J. Geophys. Res.*, *116*, A08221, doi:10.1029/2011JA016499.
Chen, L., J. Bortnik, W. Li, R. M. Thorne, and R. B. Horne (2012a), Modeling the properties of plasmaspheric hiss: 1. Dependence on chorus wave emission, *J. Geophys. Res.*, *117*, A05201, doi:10.1029/2011JA017201.
Chen, L., W. Li, J. Bortnik, and R. M. Thorne (2012b), Amplification of whistler-mode hiss inside the plasmasphere, *Geophys. Res. Lett.*, *39*, L08111, doi:10.1029/2012GL051488.
Chen, L., et al. (2014), Generation of unusually low frequency plasmaspheric hiss, *Geophys. Res. Lett.*, *41*, 5702–5709, doi:10.1002/2014GL060628.
Chum, J., and O. Santolík (2005), Propagation of whistler-mode chorus to low altitudes: Divergent ray trajectories and ground accessibility, *Ann. Geophys.*, *23*, 3727–3738, doi:10.5194/angeo-23-3727-2005.
Hayakawa, M., and S. S. Sazhin (1992), Mid-latitude and plasmaspheric HISS—A review, *Planet. Space Sci.*, *40*, 1325–1338, doi:10.1016/0032-0633(92)90089-7.
Hayosh, M., F. Němec, O. Santolík, and M. Parrot (2016), Propagation properties of quasiperiodic VLF emissions observed by the DEMETER spacecraft, *Geophys. Res. Lett.*, *43*, 1007–1014, doi:10.1002/2015GL067373.
Horne, R. B. (1989), Path-integrated growth of electrostatic waves: The generation of terrestrial myriametric radiation, *J. Geophys. Res.*, *94*(A7), 8895–8909.
Li, L. Y., J. B. Cao, J. Y. Yang, J. J. Berthelier, and J.-P. Lebreton (2015), Semiannual and solar activity variations of daytime plasma observed by DEMETER in the ionosphere-plasmasphere transition region, *J. Geophys. Res. Space Physics*, *120*, 10,640–10,653, doi:10.1002/2015JA021102.
Meredith, N. P., R. B. Horne, R. M. Thorne, D. Summers, and R. R. Anderson (2004), Substorm dependence of plasmaspheric hiss, *J. Geophys. Res.*, *109*, A06209, doi:10.1029/2004JA010387.
Omura, Y., S. Nakamura, C. A. Kletzing, D. Summers, and M. Hikishima (2015), Nonlinear wave growth theory of coherent hiss emissions in the plasmasphere, *J. Geophys. Res. Space Physics*, *120*, 7642–7657, doi:10.1002/2015JA021520.
Parrot, M., et al. (2006), The magnetic field experiment IMSC and its data processing onboard DEMETER: Scientific objectives, description and first results, *Planet. Space Sci.*, *54*, 441–455, doi:10.1016/j.pss.2005.10.015.
Poeverlein, H. (1950), Strahlwege von Radiowellen in der Ionosphare: III. Bilder theoretisch ermittelter Strahlwege, *Z. Angew. Phys.*, *2*, 152–160.
Russell, C. T., R. E. Holzer, and E. J. Smith (1969), OGO 3 observations of ELF noise in the magnetosphere: 1. Spatial extent and frequency of occurrence., *J. Geophys. Res.*, *74*, 755–777, doi:10.1029/JA074i003p00755.
Santolík, O., and M. Parrot (1998), Propagation analysis of electromagnetic waves between the helium and proton gyrofrequencies in the low-altitude auroral zone, *J. Geophys. Res.*, *103*(A9), 20,469–20,480, doi:10.1029/98JA01386.
Santolík, O., and M. Parrot (1999), Case studies on the wave propagation and polarization of ELF emissions observed by Freja around the local proton gyrofrequency, *J. Geophys. Res.*, *104*(A2), 2459–2475, doi:10.1029/1998JA900045.
Santolík, O., and M. Parrot (2000), Application of wave distribution function methods to an ELF hiss event at high latitudes, *J. Geophys. Res.*, *105*(A8), 18,885–18,894, doi:10.1029/2000JA900029.
Santolík, O., J. Chum, M. Parrot, D. A. Gurnett, J. S. Pickett, and N. Cornilleau-Wehrlin (2006a), Propagation of whistler mode chorus to low altitudes: Spacecraft observations of structured ELF hiss, *J. Geophys. Res.*, *111*, A10208, doi:10.1029/2005JA011462.
Santolík, O., F. Němec, M. Parrot, D. Lagoutte, L. Madrias, and J. J. Berthelier (2006b), Analysis methods for multi-component wave measurements on board the DEMETER spacecraft, *Planet. Space Sci.*, *54*, 512–527, doi:10.1016/j.pss.2005.10.020.
Santolík, O., J. S. Pickett, D. A. Gurnett, J. D. Menietti, B. T. Tsurutani, and O. Verkhoglyadova (2010), Survey of Poynting flux of whistler mode chorus in the outer zone, *J. Geophys. Res.*, *115*, A00F13, doi:10.1029/2009JA014925.

Smith, E. J., A. M. A. Frandsen, B. T. Tsurutani, R. M. Thorne, and K. W. Chan (1974), Plasmaspheric hiss intensity variations during magnetic storms, *J. Geophys. Res.*, *79*, 2507–2510, doi:10.1029/JA079i016p02507.

Summers, D., B. Ni, N. P. Meredith, R. B. Horne, R. M. Thorne, M. B. Moldwin, and R. R. Anderson (2008), Electron scattering by whistler-mode ELF hiss in plasmaspheric plumes, *J. Geophys. Res.*, *113*, A04219, doi:10.1029/2007JA012678.

Tao, X., J. Bortnik, and M. Friedrich (2010), Variance of transionospheric VLF wave power absorption, *J. Geophys. Res.*, *115*, A07303, doi:10.1029/2009JA015115.

Thorne, R. M., E. J. Smith, R. K. Burton, and R. E. Holzer (1973), Plasmaspheric hiss, *J. Geophys. Res.*, *78*, 1581–1596, doi:10.1029/JA078i010p01581.